Author Manuscript

Accepted for publication in a peer-reviewed journal

NIST National Institute of Standards and Technology • U.S. Department of Commerce

Published in final edited form as:

Nano Lett. 2018 April 11; 18(4): 2485–2491. doi:10.1021/acs.nanolett.8b00049.

Probing the Optical Properties and Strain-Tuning of Ultrathin $Mo_{1-x}W_xTe_2$

Ozgur Burak Aslan[‡,*,a,e], **Isha M. Datye**[‡,b], **Michal J. Mleczko**[b], **Karen Sze Cheung**[a], **Sergiy Krylyuk**[f,g], **Alina Bruma**[f], **Irina Kalish**[f], **Albert V. Davydov**[f], **Eric Pop**[*,b,c,d], **Tony F. Heinz**[*,a,e]

[a]Department of Applied Physics, Stanford University, Stanford, California 94305, United States

[b]Department of Electrical Engineering, Stanford University, Stanford, California 94305, United States

[c]Department of Materials Science and Engineering, Stanford University, Stanford, California 94305, United States

[d]Precourt Institute for Energy, Stanford University, Stanford, California 94305, United States

[e]SLAC National Accelerator Laboratory, Menlo Park, California 94025, United States

[f]Material Measurement Laboratory, National Institute of Standards and Technology, Gaithersburg, Maryland 20899, United States

[g]Theiss Research, La Jolla, California 92037, United States

Abstract

Ultrathin transition metal dichalcogenides (TMDCs) have recently been extensively investigated to understand their electronic and optical properties. Here we study ultrathin $Mo_{0.91}W_{0.09}Te_2$, a semiconducting alloy of $MoTe_2$, using Raman, photoluminescence (PL), and optical absorption measurements. $Mo_{0.91}W_{0.09}Te_2$ transitions from an indirect to a direct optical band gap in the limit of monolayer thickness, exhibiting an optical gap of 1.10 eV, very close to its $MoTe_2$ counterpart. We apply tensile strain, for the first time, to monolayer $MoTe_2$ and $Mo_{0.91}W_{0.09}Te_2$ to tune the band structure of these materials; we observe that their optical band gaps decrease by 70 meV at 2.3% uniaxial strain. The spectral widths of the PL peaks decrease with increasing strain, which we attribute to weaker exciton-phonon intervalley scattering. Strained $MoTe_2$ and $Mo_{0.91}W_{0.09}Te_2$

[*]**Corresponding Authors** oba2002@stanford.edu, tony.heinz@stanford.edu, epop@stanford.edu.

Author Contributions

The manuscript was written through contributions of all authors. All authors have given approval to the final version of the manuscript.

[‡]These authors contributed equally.

Supporting Information.

The following file is available free of charge. Growth, characterization, and preparation of samples; details on the optical measurements; Raman spectroscopy of $MoTe_2$; the rate of band gap shift with strain; the peak positions and widths of strain-dependent PL measurements on 1Ls of $MoTe_2$ and $Mo_{0.91}W_{0.09}Te_2$; strain-dependent absorption and PL measurements on 1L $Mo_{0.91}W_{0.09}Te_2$; comparison of electrical transport properties of few-layer $Mo_{0.91}W_{0.09}Te_2$ and $MoTe_2$. (PDF)

The authors declare no competing financial interest.

Certain commercial equipment, instruments, or materials are identified in this paper in order to specify the experimental procedure adequately. Such identification is not intended to imply recommendation or endorsement by the National Institute of Standards and Technology, nor is it intended to imply that the materials or equipment identified are necessarily the best available for the purpose.

extend the range of band gaps of TMDC monolayers further into the near infrared, an important attribute for potential applications in optoelectronics.

Graphical Abstract

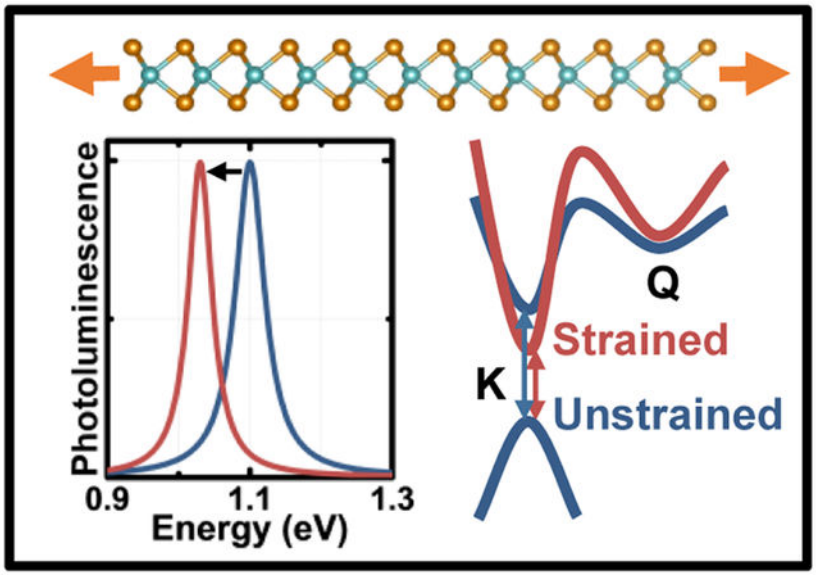

Keywords

$MoTe_2$; $MoWTe_2$; band gap; strain engineering; alloyed 2D materials; photoluminescence

Atomically thin layers of transition metal dichalcogenides (TMDCs), such as $MoTe_2$, have been extensively studied for fundamental physics and applications.[1-2] Tuning their optical properties, which can be achieved through doping, alloying, strain, and heating, is crucial for understanding their light-matter interactions and for various applications in electronics and optoelectronics. The optical properties of atomically thin $MoTe_2$ have recently been characterized experimentally,[3-7] and theoretical investigations have indicated that the aforementioned factors can significantly alter the material's band structure.[8-12] In particular, theory has predicted and measurements have demonstrated that alloying with tungsten or electrical gating of $MoTe_2$ can induce a phase change from a semiconducting to metallic state.[8-9,13-16] To date, however, few studies have experimentally examined the effects of strain on $MoTe_2$ or on $MoWTe_2$ alloys.[17]

Here we investigate $Mo_{1-x}W_xTe_2$ with $x = 0.09$ and compare the properties of this alloy with the $MoTe_2$ compound. For alloys with higher W content, *i.e.*, $x > 0.09$, all reported growth processes have produced crystals in the 1T' phase. Therefore, this composition is close to the 2H phase boundary and should exhibit the lowest threshold for inducing a 2H to 1T' phase change by an external perturbation.[15,18-19] However, the optical properties of the 2H phase of $Mo_{0.91}W_{0.09}Te_2$ have yet to be investigated in detail and compared to those of $MoTe_2$. We study atomically thin crystals of the $Mo_{0.91}W_{0.09}Te_2$ alloy by Raman scattering, photoluminescence (PL), and absorption measurements, and compare the results with those

for $MoTe_2$. We also measure PL while applying in-plane uniaxial tensile strain to the monolayer (1L) crystals of both compounds to alter their band structure, which has not been previously examined.

We have grown bulk $MoTe_2$ and $Mo_{1-x}W_xTe_2$ crystals using the chemical vapor transport (CVT) method, as detailed in the Supporting Information (SI) sections 1.1 and 1.2. The 2H crystal structure of $Mo_{0.91}W_{0.09}Te_2$ has been confirmed by powder X-ray diffraction (XRD), as shown in Figure 1a (see Figure S1 in SI section 1.3 for an extended version of the XRD data) and by scanning transmission electron microscopy (STEM) (Figure 1b). The W mole fraction in the $Mo_{1-x}W_xTe_2$ alloy, as determined from X-ray energy dispersive spectroscopy (EDS), is $x = 0.09 \pm 0.01$ (see Figure S2). For optical measurements, we have exfoliated atomically thin layers from the grown bulk $MoTe_2$ and $Mo_{0.91}W_{0.09}Te_2$ crystals (see SI section 1.4, Figure S3, and SI section 2 for details on the sample preparation and optical measurement setup).

We first perform Raman spectroscopy on $Mo_{0.91}W_{0.09}Te_2$ and $MoTe_2$ crystals exfoliated on polydimethylsiloxane (PDMS) substrates. Here and below all characterization measurements have been performed at room temperature and under ambient conditions. Figure 2 shows the Raman spectra of 1L, bilayer (2L), trilayer (3L), four-layer (4L), and bulk $Mo_{0.91}W_{0.09}Te_2$ crystals for excitation wavelengths of 532 nm, 633 nm, and 785 nm (see Figure S4 for the $MoTe_2$ spectra). We note that the relatively small band gaps of ultrathin $MoTe_2$ and $Mo_{0.91}W_{0.09}Te_2$ (see the section on PL) compared to other TMDCs enables the use of longer excitation wavelengths for resonant Raman spectroscopy.[3,20-21] We identify the following first-order Raman modes (zone-center phonons) in both materials: the out-of-plane A_{1g} (A_1' for odd, A_{1g} for even layers), in-plane E^1_{2g} (E' for odd, E_g for even layers), and out-of-plane B^1_{2g} (A_2'' for 1L, A_1' for odd, A_{1g} for even layers), which is Raman inactive in 1L and bulk crystals.[3,19,21-27] For 1L $Mo_{0.91}W_{0.09}Te_2$, the A_{1g} mode is at 172 cm^{-1} and the E^1_{2g} mode appears at 236 cm^{-1}. The weaker features at 200 cm^{-1} and 345 cm^{-1} have recently been attributed to second-order Raman processes[21] and appear to be stronger in $Mo_{0.91}W_{0.09}Te_2$ than in $MoTe_2$, possibly due to changes in the electronic structure with the addition of W.

After comparing the Raman spectra of the two materials, we observe that the A_{1g} and E^1_{2g} modes of $Mo_{0.91}W_{0.09}Te_2$ are slightly blueshifted and the B^1_{2g} mode is slightly redshifted from those of $MoTe_2$ for 1L and 2L (see Table S1 for the Raman peak positions of both materials). We explain these observations as follows. Consider a simplified linear triatomic molecule model for which interlayer interactions in the 1L and 2L have little effect (*e.g.*, no splitting of the E^1_{2g} mode). We then expect the increased W content in $Mo_{0.91}W_{0.09}Te_2$ to increase the effective mass of the transition metal atoms and to result accordingly in a redshift of modes compared to $MoTe_2$.[28] This was reported for the E^1_{2g} and B^1_{2g} modes in alloys of Mo and W dichalcogenides (*e.g.*, $Mo_{1-x}W_xS_2$ and $Mo_{1-x}W_xSe_2$).[29-33] We observe this redshift in the B^1_{2g} mode and the second-order Raman mode at 200 cm^{-1}. However, the frequency of the A_{1g} mode depends more on bond strength than on mass of the transition metal, since this atom remains stationary in this vibrational mode.[22] Since W-Te bonds are

stronger than Mo-Te bonds,[34] adding W to $MoTe_2$ stiffens the bonds, leading, as in other TMDC alloys,[31-33] to a blueshift of the A_{1g} mode. Interestingly, in contrast to other TMDC alloys,[30-33] we observe a blueshift of the E^1_{2g} mode for 1L and 2L of the alloy compared to the $MoTe_2$ crystal. This blueshift also results from the increased bond strength, which apparently outweighs the influence of the increase in mass.

Next, we examine the relative intensities of the Raman modes for different layer thicknesses in both materials. For 532 nm excitation, for both $MoTe_2$ and $Mo_{0.91}W_{0.09}Te_2$ crystals of all thicknesses, the E^1_{2g} mode is stronger than all other modes. The A_{1g} mode is strongest for 1L and becomes much weaker with increasing thickness (Figure 2a, Figure S4a). For 633 nm excitation, the A_{1g} mode is enhanced compared to the E^1_{2g} mode for 1L samples of both materials. We attribute the strength of this mode to a resonance effect associated with the excitation photon energy being close to that of the A' or B' excitons in the material (see Figure 3 for the A' and B' peak positions).[25-26] For 2L crystals, the A_{1g} and B^1_{2g} modes are comparable in intensity, but weaker than the E^1_{2g} mode. For 3L and 4L crystals, the A_{1g} mode splits into 2 peaks [$A_{1g}(R1)$ and $A_{1g}(R2)$], known as Davydov splitting,[25,35] which are stronger than the B^1_{2g} mode (see Figure 2b). The ratio of the B^1_{2g} to E^1_{2g} mode can also be used to identify thickness in few-layer crystals using both 532 and 633 nm excitation.[4,23]

Using 785 nm excitation, we observe that the E^1_{2g} mode is much weaker than the A_{1g} mode for all layer thicknesses. For the thicknesses we have measured, the A_{1g} mode is weakest for 2L and strongest for 4L crystals in both $Mo_{0.91}W_{0.09}Te_2$ and $MoTe_2$ (see Figure 2c and Figure S4c). The reason for this non-monotonic change of the intensity of the A_{1g} mode with increasing thickness is unclear. The B^1_{2g} mode does not appear in the 785 nm Raman spectra for any crystal thickness, as in the case of MoS_2 and $MoSe_2$ for excitation energies far from the C electronic resonance (see Figure 3 for the C peak position).[24,36] Calculations have shown that the A and B excitons have wave functions that are mainly confined to the individual layers,[24,36] and it has been predicted that for excitation energies near the A and B excitons, the active B^1_{2g} mode of the few-layer crystals is inactive, as it is for 1L crystals. However, the wavefunction associated with the C transition is calculated to be not confined to individual layers.[37-38] Hence, excitation nearer to the C feature, in this case 532 and 633 nm, yields Raman spectra with stronger B^1_{2g} modes. The comparisons of the Raman spectra with three different excitation wavelengths presented here provides a rapid means of determining the thickness of ultrathin layers of $Mo_{0.91}W_{0.09}Te_2$ and $MoTe_2$.

We have performed PL measurements in order to study the band structure of $Mo_{0.91}W_{0.09}Te_2$. Figure 3a displays the PL spectra of 1L to 4L and bulk $Mo_{0.91}W_{0.09}Te_2$ supported on PDMS substrates. We see that the PL intensity decreases, the peak position redshifts, and the spectral width (full width at half maximum) increases with increasing layer thickness. The 1L spectrum exhibits a single emission peak, with the maximum located at 1.10 eV and a width of 48 meV. The width of the 2L is 20 meV greater than that of the 1L. For the bulk, we find a much broader and weaker PL feature peaked at 0.98 eV.

In order to comment on the nature of the peaks observed in the PL spectra and understand the changes with increasing material thickness, we have also measured the reflection contrast ($\Delta R/R$) spectra of 1L to 3L $Mo_{0.91}W_{0.09}Te_2$ on PDMS substrates, as displayed in Figure 3b, to probe their absorption spectra (see SI section 2 for details on the reflection contrast measurements). We expect to observe only direct optical transitions in the reflection contrast spectrum since the indirect transitions produce only weak contributions to the absorption spectrum. Several features are observed in the spectra of Figure 3b, and we expect them to arise from mechanisms similar to those in $MoTe_2$. Thus, we have labeled them according to the bulk assignments of Wilson and Yoffe[39] as was previously done for the case of $MoTe_2$.[3] These spectroscopic features are associated with transitions in different parts of the Brillouin zone of $Mo_{0.91}W_{0.09}Te_2$. The *A*, *B* and *A*′, *B*′ pairs have been identified as excitonic transitions with the *A*-*B* splitting arising from spin-orbit interactions.[39-40] As for other TMDC monolayers, the *A* and *B* peaks are assigned to excitonic peaks associated with the lowest direct optical transition at the *K*-point.[41-43] The *C* and *D* features have been attributed to regions of parallel bands near the *Γ* point of the Brillouin zone of bulk $MoTe_2$[44] and to similar parallel bands in monolayers of other TMDCs.[37,45]

We now compare the PL and reflection contrast response of $Mo_{0.91}W_{0.09}Te_2$ for different thicknesses. Figure 3b shows that the reflection contrast increases and the *A* exciton redshifts with increasing thickness. The PL spectra in Figure 3a show that the peak position also redshifts; however, the rate of the redshift of the PL peak is faster than that of the *A* exciton and the intensity of the PL peak decreases as opposed to that of the *A* exciton. We report the position of the *A* exciton and the PL peak position as a function of thickness in Figure 3c. The *A* exciton redshifts by 33 meV to 1.067 eV from 1L to 2L and continues shifting gradually with increasing thickness. However, the PL peaks redshift more than the *A* exciton peaks; the two peaks are separated by 5 meV for 1L, but by 45 meV for 4L.

We attribute this large difference in the shift between the absorption and emission features to the emergence of an indirect transition at lower energies than the *A* exciton with increasing thickness, as observed in other semiconducting TMDCs.[46-47] We expect the indirect band gap to contribute to PL, but not significantly to the absorption spectrum. We thus conclude that 1L $Mo_{0.91}W_{0.09}Te_2$ exhibits a direct band gap, unlike the crystals thicker than 2L, in accordance with the behavior of its $MoTe_2$ counterpart. The PL intensity of the 1L crystal is about three orders of magnitude greater than that of the bulk, due to the direct optical gap transition of the former. Even though the PL intensity is significantly weaker for 2L than it is for 1L, since the PL peak and the *A* exciton are separated by only 10 meV, the assignment of the 2L material as indirect gap is unclear. However, the 20 meV increase in the width of the PL and *A* exciton peaks of 2L as compared to 1L strongly indicates the presence of a scattering channel for the *A* exciton in the 2L. We also note that there have been different opinions on the nature of the 2L $MoTe_2$ band gap, both at room[3,5] and low temperatures.[4]

The near-IR part of the 1L absorption spectrum is shown in greater detail in Figure 3d. We find that the *A* and B features are located at 1.10 eV and 1.38 eV, respectively. The corresponding features appear at similar energies of 1.10 eV and 1.35 eV, respectively, for 1L $MoTe_2$.[3] We note that the direct gap, or *A* exciton, position in $Mo_{0.91}W_{0.09}Te_2$ is not very different from that of $MoTe_2$, which is compatible with the fact that for a given

chalcogen (S, Se), the band gaps of Mo and W dichalcogenides are quite similar.[20] The *A*-*B* splitting for 1L is found to be 276 meV, which is slightly greater than the $MoTe_2$ value of 250 meV.[3] We attribute this increase to the presence of W, since dichalcogenides of W have significantly higher *A*-*B* splitting than those of Mo.[20,48-49] Thus, our PL and reflection measurements have revealed that 2H $Mo_{0.91}W_{0.09}Te_2$ is a semiconducting material like 2H $MoTe_2$.

To gain further insight into the band structure of 1L $MoTe_2$ and $Mo_{0.91}W_{0.09}Te_2$, we perform strain-dependent PL measurements on these materials. We apply uniaxial in-plane tensile strain to a flexible substrate using a two-point bending apparatus (see SI section 1.4 and Figure S3 for more details). We used PEN (polyethylene naphthalate) or PETG (polyethylene terephthalate glycol-modified) instead of PDMS for the bending platform (Figure S3), due to their higher Young's modulus. Figure 4a-b shows the PL measurements of 1L $Mo_{0.91}W_{0.09}Te_2$ and $MoTe_2$ as a function of strain. As the strain increases, the PL peak redshifts, corresponding to a decrease in the band gap. For $Mo_{0.91}W_{0.09}Te_2$, the PL peak shifts from 1.09 eV at 0% strain to 1.02 eV at 2.3% strain or −30 meV/% strain. For $MoTe_2$, the PL peak shifts from 1.08 eV at 0% strain to 1.01 eV at 2.1% strain or −33 meV/% strain. We note that these values of strain and peak shift with strain are reasonable, as discussed in SI section 4 and shown in Figure S5. The widths of the $Mo_{0.91}W_{0.09}Te_2$ and $MoTe_2$ PL peaks decrease from 63 meV and 59 meV, respectively, at 0% strain to minimum values of 49 meV and 42 meV, respectively, with strain. Figure 4c shows how the 1L $MoTe_2$ PL peak energy and spectral widths vary with strain (see SI Figure S6a for the $Mo_{0.91}W_{0.09}Te_2$ results).

To account for the unexpected decrease of the width of the emission peak in the PL spectra with increasing strain for both materials, we can identify three possible factors: 1) the contribution to PL from trions is suppressed, 2) the material conforms better to the flexible substrate (after being transferred), reducing inhomogeneous broadening, or 3) exciton-phonon scattering is partially suppressed.

We first consider the suppression of trion emission due to strain. Trions are not expected to contribute much to absorption unless the sample is heavily doped.[50-51] However, trions can still contribute appreciably to PL since they are more stable even at room temperature due to their high binding energy of about 25 meV.[6-7] Therefore, if suppression of trion PL caused the reduction in the linewidth, we would not expect to see a parallel narrowing in the absorption feature with strain. However, our measurements show a similar decrease in the width of the absorption and PL features, thus ruling out this mechanism (see SI section 6 and Figures S7 and S8).

Second, we consider the possibility that the material conforms better to the substrate under strain, leading to a reduction of inhomogeneous broadening. We first observe that the width of the emission feature of strained 1Ls drops to a value as low as 42 meV (Figure 4c), which is less than that of any as-exfoliated samples (for which the width is around 47-50 meV).[3,5] Further, similar measurements on 1L WSe_2 by Schmidt *et al.* have demonstrated that the strain-induced narrowing of the spectral widths is reversible upon the release of strain.[52] This observation suggests that the elimination of inhomogeneities alone cannot account for

line narrowing in their case, as the inhomogeneities are not expected to recover fully when the strain is released. Hence, we do not expect this mechanism to explain our observations.

Third, we consider the effect of strain on the exciton-phonon coupling. As we know from the current and earlier studies, 1Ls of both materials have direct optical gaps.[3-5,53] However, the 1L has an indirect transition at a slightly higher energy than that of the A exciton, which is known from band structure calculations and from extrapolating the energy of the indirect gap as compared to that of 2L and thicker crystals.[3-5,53] Moreover, the energy separation between the minima of indirect Q (also known as T)[54-55] and direct K valleys, ΔE_{QK}, in the conduction band will increase with uniaxial (as well as biaxial) strain in similar material systems.[11-12,56-58] This is illustrated in Figure 4d, which shows a schematic band structure of strained and unstrained 1L $MoTe_2$. However, scattering of an electron from the K to Q valley requires the absorption of a phonon. This becomes less likely with increasing ΔE_{QK}. Therefore, we infer from our results that a weakening in the exciton-phonon intervalley scattering is mainly responsible for the decrease in the spectral linewidths. We attribute at least 6 meV of the width of the emission feature in the unstrained material to the exciton-phonon scattering from K to Q (Γ_{QK}). We also estimate an upper limit of 110 fs for the lifetime of the exciton-phonon scattering from K to Q in 1L $MoTe_2$ and $Mo_{0.91}W_{0.09}Te_2$ (see SI section 6). The ability to suppress phonon absorption indicates that Q and K states are within a few times the phonon energy and the highest energy phonon to mediate such scattering [the $LO(E')$ mode] is about 30 meV.[21,54,59] Thus, we predict that ΔE_{QK} of the unstrained 1Ls is not much larger than 30 meV. We expect the linewidth narrowing effect via tensile strain to be smaller (larger) for MoS_2 (WSe_2 and WS_2), for which ΔE_{QK} is predicted to be larger (smaller) than that in $MoTe_2$.[54,59]

Here we note an advantage of a strain-dependent study over a temperature-dependent one. Strain, like temperature, can modify the band structure, but in the former case without significantly affecting the population of phonons. We also note that it is typically assumed that the relative energy of different valleys is not affected by temperature. This is not always correct as lowering the temperature has a similar effect to biaxial compressive strain.[60] Therefore, tuning the bands of nearly direct or indirect gap semiconductors via strain will provide more insight about the band structure and can help interpret the temperature-dependent studies on the spectral linewidths of TMDCs.[6,52,61-62]

Finally, we would like to consider the implications of weaker exciton-phonon scattering for electron transport. There have been calculations of the enhancement of transport properties in group VI TMDCs due to the change in the relative energies of K and Q valleys in the conduction band under tensile strain, leading to a reduction in electron-phonon scattering.[11,63] We propose that this effect should be larger for $MoTe_2$ than MoS_2, as the former has a smaller value for ΔE_{QK}. A similar phenomenon has been exploited to enhance the electron mobility of silicon transistors, where the intervalley energy separation increases with tensile strain, leading to reduced intervalley electron-phonon scattering.[64-65]

In summary, we have characterized single-crystal 2H $Mo_{0.91}W_{0.09}Te_2$ down to monolayer thickness with photoluminescence, absorption, and Raman spectroscopy. We have determined that atomically thin 2H $Mo_{0.91}W_{0.09}Te_2$ is a semiconductor with similar optical

properties to $MoTe_2$; the monolayer possesses a direct optical band gap at 1.10 eV, and the thicker layers become indirect. The presence of W in the alloy alters the band structure, as observed by absorption measurements, and can be studied further by Raman spectroscopy, particularly using resonant excitation.[66] Given that this alloy is closest in W-content to the 2H to 1T' phase transition,[19] it may be a promising material for phase-change memory applications. We have manipulated the band structure of monolayer $MoTe_2$ and $Mo_{0.91}W_{0.09}Te_2$ via tensile strain up to 2.3% and have thereby lowered the optical band gap of these materials to near 1 eV. We have thus extended the optical range of group VI TMDC monolayers further into the near-infrared (NIR) region. We have also observed that the relative energy separation between valleys changes with strain, and that exciton-phonon intervalley scattering can also be manipulated in this fashion. We attribute the reduced spectral linewidth of the *A* exciton under tensile strain to a decrease in the rate of exciton-phonon scattering. This suggests a corresponding decrease in the electron-phonon scattering rate and a potential improvement in the electrical transport properties in these materials with tensile strain.

Supplementary Material

Refer to Web version on PubMed Central for supplementary material.

ACKNOWLEDGMENTS

We thank Ian Fisher and Hsueh-Hui Kuo for the $MoTe_2$ growth, and Ali Dadgar for useful discussions. This work was supported in part by the Army Research Office (ARO) Grant W911NF-15-1-0570, the Air Force Office of Scientific Research (AFOSR) Grants FA9550-14-1-0251 and FA9550-14-1-0040 (O.B.A.), the National Science Foundation EFRI 2-DARE Grant 1542883, the Initiative for Nanoscale Materials and Processes (INMP), and the Department of Energy, Office of Science, Basic Energy Sciences, Materials Sciences and Engineering Division under Contract DE-AC02-76SF00515 (T.F.H.). S.K. acknowledges support from the U.S. Department of Commerce, National Institute of Standards and Technology under financial assistance award 70NANB16H043. I.M.D. also acknowledges support from the NDSEG graduate fellowship.

REFERENCES

(1). Novoselov KS; Jiang D; Schedin F; Booth TJ; Khotkevich VV; Morozov SV; Geim AK Two-Dimensional Atomic Crystals. Proc. Natl. Acad. Sci. U.S.A 2005, 102, 10451–3. [PubMed: 16027370]

(2). Chhowalla M; Shin HS; Eda G; Li LJ; Loh KP; Zhang H The chemistry of two-dimensional layered transition metal dichalcogenide nanosheets. Nature Chem. 2013, 5, 263–75. [PubMed: 23511414]

(3). Ruppert C; Aslan OB; Heinz TF Optical Properties and Band Gap of Single- and Few-layer $MoTe_2$ Crystals. Nano Lett. 2014, 14, 6231–6. [PubMed: 25302768]

(4). Lezama IG; Arora A; Ubaldini A; Barreteau C; Giannini E; Potemski M; Morpurgo AF Indirect-to-Direct Band Gap Crossover in Few-Layer $MoTe_2$. Nano Lett. 2015, 15, 2336–42. [PubMed: 25803208]

(5). Froehlicher G; Lorchat E; Berciaud S Direct versus indirect band gap emission and exciton-exciton annihilation in atomically thin molybdenum ditelluride ($MoTe_2$). Phys. Rev. B 2016, 94, 085429.

(6). Koirala S; Mouri S; Miyauchi Y; Matsuda K Homogeneous linewidth broadening and exciton dephasing mechanism in $MoTe_2$. Phys. Rev. B 2016, 93, 075411.

(7). Yang J; Lu TY; Myint YW; Pei JJ; Macdonald D; Zheng JC; Lu YR Robust Excitons and Trions in Monolayer $MoTe_2$. ACS Nano 2015, 9, 6603–9. [PubMed: 26039551]

(8). Li Y; Duerloo KAN; Wauson K; Reed EJ Structural semiconductor-to-semimetal phase transition in two-dimensional materials induced by electrostatic gating. Nat. Commun 2016, 7, 10671. [PubMed: 26868916]

(9). Duerloo KAN; Reed EJ Structural Phase Transitions by Design in Monolayer Alloys. ACS Nano 2016, 10, 289–97. [PubMed: 26647117]

(10). Duerloo KAN; Li Y; Reed EJ Structural phase transitions in two-dimensional Mo- and W-dichalcogenide monolayers. Nat. Commun 2014, 5, 4214. [PubMed: 24981779]

(11). Hosseini M; Elahi M; Pourfath M; Esseni D Very large strain gauges based on single layer $MoSe_2$ and WSe_2 for sensing applications. Appl. Phys. Lett 2015, 107, 253503.

(12). Villegas CEP; Rocha AR Elucidating the Optical Properties of Novel Heterolayered Materials Based on $MoTe_2$-InN for Photovoltaic Applications. J. Phys. Chem. C 2015, 119, 11886–95.

(13). Berry J; Zhou SS; Han J; Srolovitz DJ; Haataja MP Dynamic Phase Engineering of Bendable Transition Metal Dichalcogenide Monolayers. Nano Lett. 2017, 17, 2473–81. [PubMed: 28281764]

(14). Zhang C; Kc S; Nie Y; Liang C; Vandenberghe WG; Longo RC; Zheng Y; Kong F; Hong S; Wallace RM; Cho K Charge Mediated Reversible Metal–Insulator Transition in Monolayer $MoTe_2$ and $W_xMo_{1-x}Te_2$ Alloy. ACS Nano 2016, 10, 7370–5. [PubMed: 27415610]

(15). Rhodes D; Chenet DA; Janicek BE; Nyby C; Lin Y; Jin W; Edelberg D; Mannebach E; Finney N; Antony A; Schiros T; Klarr T; Mazzoni A; Chin M; Chiu YC; Zheng W; Zhang QR; Ernst F; Dadayp JI; Tong X; Ma J; Lou R; Wan S; Qian T; Ding H; Osgood RM; Paley DW; Lindenberg AM; Huang PY; Pasupathy AN; Dubey M; Hone J; Balicas L Engineering the Structural and Electronic Phases of $MoTe_2$ through W Substitution. Nano Lett. 2017, 17, 1616–22. [PubMed: 28145719]

(16). Wang Y; Xiao J; Zhu H; Li Y; Alsaid Y; Fong KY; Zhou Y; Wang S; Shi W; Wang Y; Zettl A; Reed EJ; Zhang X Structural phase transition in monolayer $MoTe_2$ driven by electrostatic doping. Nature 2017, 550, 487–91. [PubMed: 29019982]

(17). Song S; Keum DH; Cho S; Perello D; Kim Y; Lee YH Room Temperature Semiconductor-Metal Transition of $MoTe_2$ Thin Films Engineered by Strain. Nano Lett. 2016, 16, 188–93. [PubMed: 26713902]

(18). Lv YY; Cao L; Li X; Zhang BB; Wang K; Pang B; Ma LG; Lin DJ; Yao SH; Zhou J; Chen YB; Dong ST; Liu WC; Lu MH; Chen YL; Chen YF Composition and temperature-dependent phase transition in miscible $Mo_{1-x}W_xTe_2$ single crystals. Sci. Rep 2017, 7, 44587. [PubMed: 28294191]

(19). Oliver SM; Beams R; Krylyuk S; Kalish I; Singh AK; Bruma A; Tavazza F; Joshi J; Stone IR; Stranick SJ; Davydov AV; Vora PM The structural phases and vibrational properties of $Mo_{1-x}W_xTe_2$ alloys. 2D Mater. 2017, 4, 045008.

(20). Li Y; Chernikov A; Zhang X; Rigosi A; Hill HM; van der Zande AM; Chenet DA; Shih E-M; Hone J; Heinz TF Measurement of the optical dielectric function of monolayer transition-metal dichalcogenides: MoS_2, $MoSe_2$, WS_2, and WSe_2. Phys. Rev. B 2014, 90, 205422.

(21). Guo HH; Yang T; Yamamoto M; Zhou L; Ishikawa R; Ueno K; Tsukagoshi K; Zhang ZD; Dresselhaus MS; Saito R Double resonance Raman modes in monolayer and few-layer $MoTe_2$. Phys. Rev. B 2015, 91, 205415.

(22). Luo X; Zhao Y; Zhang J; Toh M; Kloc C; Xiong Q; Quek SY Effects of lower symmetry and dimensionality on Raman spectra in two-dimensional WSe_2. Phys. Rev. B 2013, 88, 195313.

(23). Yamamoto M; Wang ST; Ni MY; Lin YF; Li SL; Aikawa S; Jian WB; Ueno K; Wakabayashi K; Tsukagoshi K Strong Enhancement of Raman Scattering from a Bulk-Inactive Vibrational Mode in Few-Layer $MoTe_2$. ACS Nano 2014, 8, 3895–903. [PubMed: 24654654]

(24). Scheuschner N; Gillen R; Staiger M; Maultzsch J Interlayer resonant Raman modes in few-layer MoS_2. Phys. Rev. B 2015, 91, 235409.

(25). Song QJ; Tan QH; Zhang X; Wu JB; Sheng BW; Wan Y; Wang XQ; Dai L; Tan PH Physical origin of Davydov splitting and resonant Raman spectroscopy of Davydov components in multilayer $MoTe_2$. Phys. Rev. B 2016, 93, 115409.

(26). Grzeszczyk M; Golasa K; Zinkiewicz M; Nogajewski K; Molas MR; Potemski M; Wysmolek A; Babinski A Raman scattering of few-layers $MoTe_2$. 2D Mater. 2016, 3, 025010.

(27). Gołasa K; Grzeszczyk M; Molas MR; Zinkiewicz M; Bala Ł; Nogajewski K; Potemski M; Wysmołek A; Babiński A Resonant quenching of Raman scattering due to out-of-plane A_{1g}/A'_1 modes in few-layer $MoTe_2$. Nanophotonics 2017, 6, 1281–8.

(28). Landau LD; Lifshitz EM, Mechanics. 2nd ed.; Pergamon: Bristol, UK, 1969.

(29). Terrones H; Corro ED; Feng S; Poumirol JM; Rhodes D; Smirnov D; Pradhan NR; Lin Z; Nguyen MAT; Elías AL; Mallouk TE; Balicas L; Pimenta MA; Terrones M New First Order Raman-Active Modes in Few Layered Transition Metal Dichalcogenides. Sci. Rep 2014, 4, 4215. [PubMed: 24572993]

(30). Qiao X-F; Li X-L; Zhang X; Shi W; Wu J-B; Chen T; Tan P-H Substrate-free layer-number identification of two-dimensional materials: A case of $Mo_{0.5}W_{0.5}S_2$ alloy. Appl. Phys. Lett 2015, 106, 223102.

(31). Wei-Jhih S; Wei-Qian W; You-Li W; Wan-Siang G; Shin-ichi H; Ruei-San C; Ying-Sheng H; Kuei-Yi L $Mo_{1-x}W_xS_2$-based photodetector fabrication and photoconductive characteristics. Jpn. J. Appl. Phys 2017, 56, 032201.

(32). Zhang M; Wu J; Zhu Y; Dumcenco DO; Hong J; Mao N; Deng S; Chen Y; Yang Y; Jin C; Chaki SH; Huang Y-S; Zhang J; Xie L Two-Dimensional Molybdenum Tungsten Diselenide Alloys: Photoluminescence, Raman Scattering, and Electrical Transport. ACS Nano 2014, 8, 7130–7. [PubMed: 24884059]

(33). Chen Y; Dumcenco DO; Zhu Y; Zhang X; Mao N; Feng Q; Zhang M; Zhang J; Tan P-H; Huang Y-S; Xie L Composition-dependent Raman modes of $Mo_{1-x}W_xS_2$ monolayer alloys. Nanoscale 2014, 6, 2833–9. [PubMed: 24469100]

(34). Huang L-F; Zeng Z Roles of Mass, Structure, and Bond Strength in the Phonon Properties and Lattice Anharmonicity of Single-Layer Mo and W Dichalcogenides. J. Phys. Chem. C 2015, 119, 18779–89.

(35). Froehlicher G; Lorchat E; Fernique F; Joshi C; Molina-Sanchez A; Wirtz L; Berciaud S Unified Description of the Optical Phonon Modes in N-Layer $MoTe_2$. Nano Lett. 2015, 15, 6481–9. [PubMed: 26371970]

(36). Soubelet P; Bruchhausen AE; Fainstein A; Nogajewski K; Faugeras C Resonance effects in the Raman scattering of monolayer and few-layer $MoSe_2$. Phys. Rev. B 2016, 93, 155407.

(37). Qiu DY; da Jornada FH; Louie SG Optical Spectrum of MoS_2: Many-Body Effects and Diversity of Exciton States. Phys. Rev. Lett. 2013, 111, 216805. [PubMed: 24313514]

(38). Gillen R; Maultzsch J Light-Matter Interactions in Two-Dimensional Transition Metal Dichalcogenides: Dominant Excitonic Transitions in Mono- and Few-Layer MoX_2 and Band Nesting. IEEE J. Sel. Topics Quantum Electron 2017, 23, 9000512.

(39). Wilson JA; Yoffe AD The transition metal dichalcogenides discussion and interpretation of the observed optical, electrical and structural properties. Adv. Phys 1969, 18, 193–335.

(40). Beal AR; Liang WY; Knights JC Transmission spectra of some transition metal dichalcogenides: II. Group VIA: trigonal prismatic coordination. J. Phys. C: Solid State Phys 1972, 5, 3540.

(41). Zhang Y; Chang TR; Zhou B; Cui YT; Yan H; Liu Z; Schmitt F; Lee J; Moore R; Chen Y; Lin H; Jeng HT; Mo SK; Hussain Z; Bansil A; Shen ZX Direct observation of the transition from indirect to direct bandgap in atomically thin epitaxial $MoSe_2$. Nat. Nanotech 2014, 9, 111–5.

(42). Yun WS; Han SW; Hong SC; Kim IG; Lee JD Thickness and strain effects on electronic structures of transition metal dichalcogenides: 2H-MX_2 semiconductors (M = Mo, W; X = S, Se, Te). Phys. Rev. B 2012, 85, 033305.

(43). Jin WC; Yeh PC; Zaki N; Zhang DT; Sadowski JT; Al-Mahboob A; van der Zande AM; Chenet DA; Dadap JI; Herman IP; Sutter P; Hone J; Osgood RM Direct Measurement of the Thickness-Dependent Electronic Band Structure of MoS_2 Using Angle-Resolved Photoemission Spectroscopy. Phys. Rev. Lett 2013, 111, 106801. [PubMed: 25166690]

(44). Bromley RA M. RB; Yoffe AD The band structures of some transition metal dichalcogenides. III. Group VIA: trigonal prism materials. J. Phys. C Solid State Phys 1972, 5, 759.

(45). Carvalho A; Ribeiro RM; Neto AHC Band nesting and the optical response of two-dimensional semiconducting transition metal dichalcogenides. Phys. Rev. B 2013, 88, 115205.

(46). Mak KF; Lee C; Hone J; Shan J; Heinz TF Atomically Thin MoS_2: A New Direct-Gap Semiconductor. Phys. Rev. Lett 2010, 105, 136805. [PubMed: 21230799]

(47). Zhao W; Ghorannevis Z; Chu L; Toh M; Kloc C; Tan P-H; Eda G Evolution of Electronic Structure in Atomically Thin Sheets of WS_2 and WSe_2. ACS Nano 2013, 7, 791–7. [PubMed: 23256505]

(48). Liu GB; Shan WY; Yao YG; Yao W; Xiao D Three-band tight-binding model for monolayers of group-VIB transition metal dichalcogenides. Phys. Rev. B 2013, 88, 085433.

(49). Rigosi AF; Hill HM; Rim KT; Flynn GW; Heinz TF Electronic band gaps and exciton binding energies in monolayer $Mo_xW_{1-x}S_2$ transition metal dichalcogenide alloys probed by scanning tunneling and optical spectroscopy. Phys. Rev. B 2016, 94, 075440.

(50). Mak KF; He K; Lee C; Lee GH; Hone J; Heinz TF; Shan J Tightly bound trions in monolayer MoS_2. Nat. Mater 2013, 12, 207–11. [PubMed: 23202371]

(51). Chernikov A; van der Zande AM; Hill HM; Rigosi AF; Velauthapillai A; Hone J; Heinz TF Electrical Tuning of Exciton Binding Energies in Monolayer WS_2. Phys. Rev. Lett 2015, 115, 126802. [PubMed: 26431003]

(52). Schmidt R; Niehues I; Schneider R; Druppel M; Deilmann T; Rohlfing M; de Vasconcellos SM; Castellanos-Gomez A; Bratschitsch R Reversible uniaxial strain tuning in atomically thin WSe_2. 2D Mater. 2016, 3, 021011.

(53). Robert C; Picard R; Lagarde D; Wang G; Echeverry JP; Cadiz F; Renucci P; Hogele A; Amand T; Marie X; Gerber IC; Urbaszek B Excitonic properties of semiconducting monolayer and bilayer $MoTe_2$. Phys. Rev. B 2016, 94, 155425.

(54). Jin ZH; Li XD; Mullen JT; Kim KW Intrinsic transport properties of electrons and holes in monolayer transition-metal dichalcogenides. Phys. Rev. B 2014, 90, 045422.

(55). Herring C Character tables for two space groups. J. Franklin Inst 1942, 233, 525–43.

(56). Rhim SH; Kim YS; Freeman AJ Strain-induced giant second-harmonic generation in monolayered 2H-MoX_2 (X = S, Se, Te). Appl. Phys. Lett 2015, 107, 241908.

(57). Chang CH; Fan XF; Lin SH; Kuo JL Orbital analysis of electronic structure and phonon dispersion in MoS_2, $MoSe_2$, WS_2, and WSe_2 monolayers under strain. Phys. Rev. B 2013, 88, 195420.

(58). Shi HL; Pan H; Zhang YW; Yakobson BI Quasiparticle band structures and optical properties of strained monolayer MoS_2 and WS_2. Phys. Rev. B 2013, 87, 155304.

(59). Kormanyos A; Burkard G; Gmitra M; Fabian J; Zolyomi V; Drummond ND; Fal'ko V k.p theory for two-dimensional transition metal dichalcogenide semiconductors. 2D Mater. 2015, 2, 022001.

(60). Wang ZY; Zhou YL; Wang XQ; Wang F; Sun Q; Guo ZX; Jia Y Effects of in-plane stiffness and charge transfer on thermal expansion of monolayer transition metal dichalcogenide. Chin. Phys. B 2015, 24, 026501.

(61). Selig M; Berghauser G; Raja A; Nagler P; Schuller C; Heinz TF; Korn T; Chernikov A; Malic E; Knorr A Excitonic linewidth and coherence lifetime in monolayer transition metal dichalcogenides. Nat. Commun 2016, 7, 13279. [PubMed: 27819288]

(62). Zhang CD; Chen YX; Johnson A; Li MY; Li LJ; Mende PC; Feenstra RM; Shih CK Probing Critical Point Energies of Transition Metal Dichalcogenides: Surprising Indirect Gap of Single Layer WSe_2. Nano Lett. 2015, 15, 6494–500. [PubMed: 26389585]

(63). Ge YF; Wan WH; Feng WX; Xiao D; Yao YG Effect of doping and strain modulations on electron transport in monolayer MoS_2. Phys. Rev. B 2014, 90, 035414.

(64). Takagi SI; Hoyt JL; Welser JJ; Gibbons JF Comparative study of phonon-limited mobility of two-dimensional electrons in strained and unstrained Si metal-oxide-semiconductor field-effect transistors. J. Appl. Phys 1996, 80, 1567–77.

(65). Fischetti MV; Laux SE Band structure, deformation potentals, and carrier mobility in strained Si, Ge, and SiGe alloys. J. Appl. Phys 1996, 80, 2234–52.

(66). del Corro E; Terrones H; Elias A; Fantini C; Feng SM; Nguyen MA; Mallouk TE; Terrones M; Pimenta MA Excited Excitonic States in 1L, 2L, 3L, and Bulk WSe_2 Observed by Resonant Raman Spectroscopy. ACS Nano 2014, 8, 9629–35. [PubMed: 25162682]

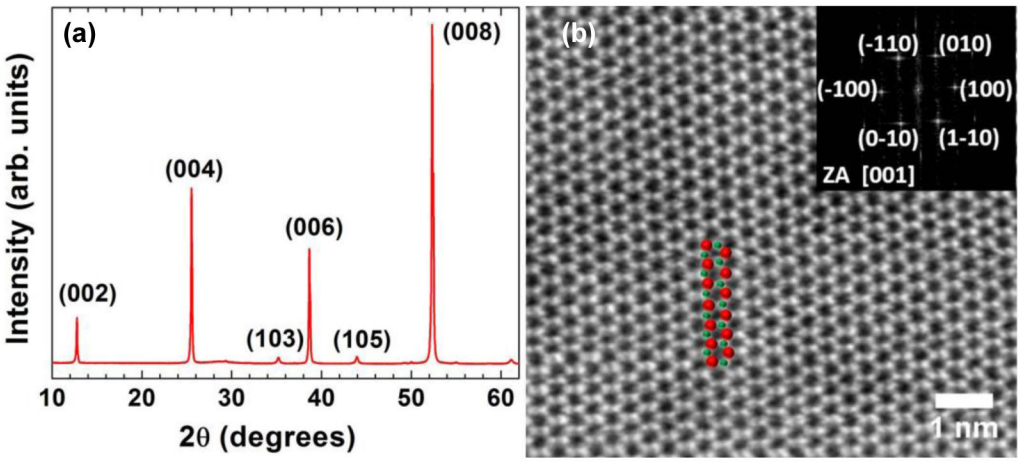

Figure 1.

(a) Powder XRD pattern of 2H-$Mo_{0.91}W_{0.09}Te_2$. (b) High angle annular dark field scanning electron microscopy (HAADF-STEM) image of a 2H $Mo_{0.91}W_{0.09}Te_2$ sample together with an overlapped structural model; red (large) spheres: Mo/W atoms; green (small) spheres: Te atoms. Inset: Fast Fourier Transform (FFT) emphasizing the [001] zone axis.

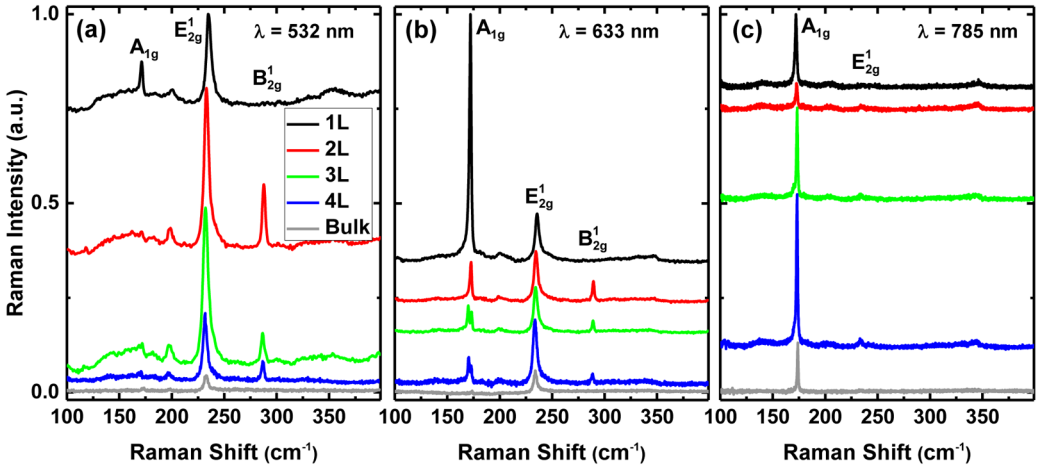

Figure 2.

Raman spectra of 1L to 4L and bulk $Mo_{0.91}W_{0.09}Te_2$ (modes labeled according to bulk notation) for excitation wavelengths of (a) 532 nm, (b) 633 nm, and (c) 785 nm. The spectra are vertically offset for clarity.

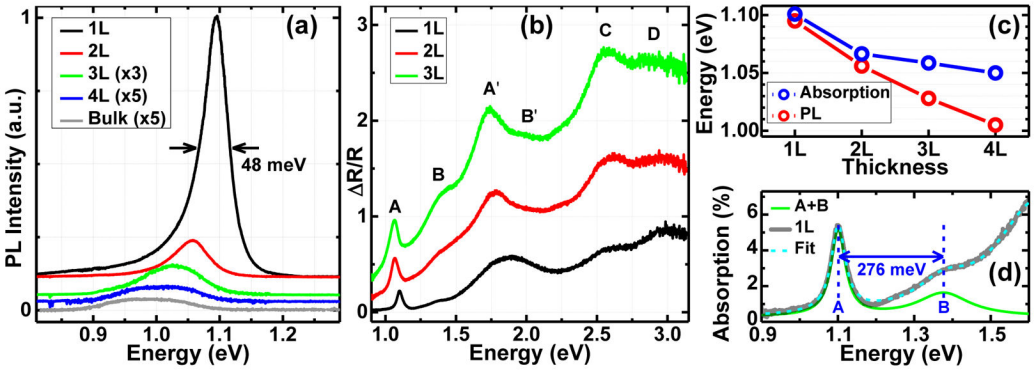

Figure 3.

(a) PL spectra of 1L to 4L and bulk $Mo_{0.91}W_{0.09}Te_2$. 1L to 4L spectra are vertically offset for clarity. Black arrows indicate the width of 48 meV of the 1L spectrum. (b) Reflection contrast ($\Delta R/R$) spectra for 1L to 3L $Mo_{0.91}W_{0.09}Te_2$. (c) Comparison of the *A* exciton and PL peak positions as a function of crystal thickness. (d) Absorption spectrum for the 1L in the near-IR, shown in terms of absorption for a free-standing layer. The green curve shows the contributions of the *A* and *B* excitons to the spectrum based on a fit (dotted line) to the experimental data.

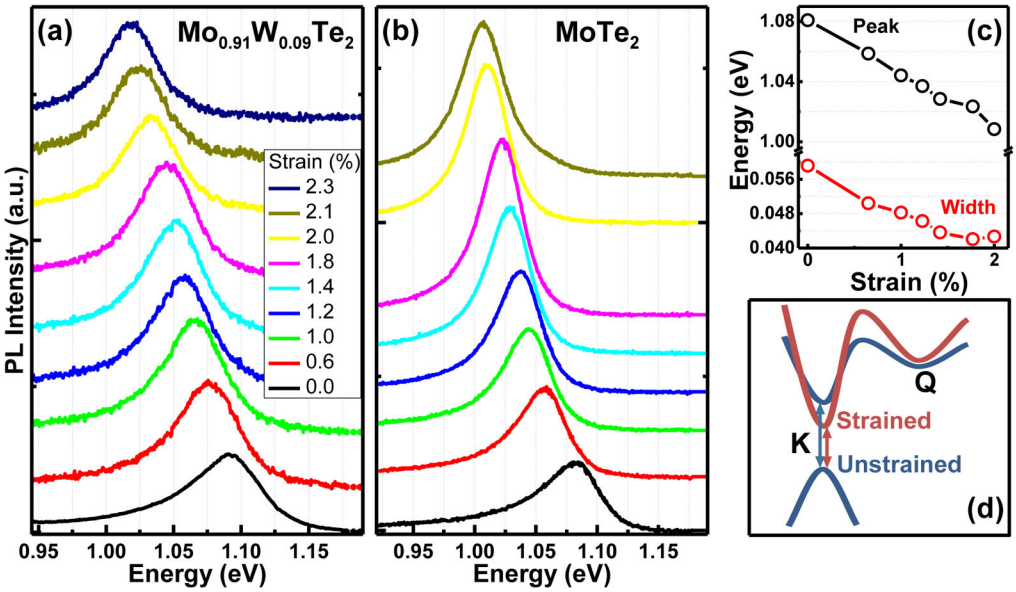

Figure 4.

PL spectra of 1L (a) $Mo_{0.91}W_{0.09}Te_2$ and (b) $MoTe_2$ under different amounts of uniaxial tensile strain. All spectra are vertically offset for clarity. (c) The dependence of the peak energy and spectral width of 1L $MoTe_2$ on strain. (d) Schematic band structure of strained and unstrained 1L $MoTe_2$, showing changes in the energy separation between the minima of the *K* and *Q* valleys in the conduction band.